A Universal Approach to Coverage Probability and Throughput Analysis for Cellular Networks

Hui Zhang, Sheng Chen, *Fellow, IEEE*, Liang Feng, Yifeng Xie, and Lajos Hanzo, *Fellow, IEEE*

***Abstract*—This paper proposes a novel tractable approach for accurately analyzing both the coverage probability and the achievable throughput of cellular networks. Specifically, we derive a new procedure referred to as the equivalent uniform-density plane-entity (EUDPE) method for evaluating the other-cell interference. Furthermore, we demonstrate that our EUDPE method provides a universal and effective means to carry out the lower bound analysis of both the coverage probability and the average throughput for various base-station distribution models that can be found in practice, including the stochastic Poisson point process (PPP) model, a uniformly and randomly distributed model, and a deterministic grid-based model. The lower bounds of coverage probability and average throughput calculated by our proposed method agree with the simulated coverage probability and average throughput results and those obtained by the existing PPP-based analysis, if not better. Moreover, based on our new definition of cell edge boundary, we show that the cellular topology with randomly distributed base stations (BSs) only tends toward the Voronoi tessellation when the path-loss exponent is sufficiently high, which reveals the limitation of this popular network topology.**

***Index Terms*—Achievable throughput, cellular coverage, cellular networks, deterministic grid-based model, Poisson point process (PPP) model, uniformly and randomly distributed model.**

I. Introduction

SINCE cellular systems are under growing pressure to increase the volume of data delivered to consumers, establishing an accurate performance prediction model is of prime significance [1]. Cellular systems are evolving into a large-scale heterogeneous network architecture, constructed by overlapping network tiers, such as macrocells, picocells, femtocells, etc. [2]–[4]. The traditional cellular analysis relying on an idealized hexagonal model does not realistically represent the actual distribution of cells. Clearly, such a simplistic model cannot be used for accurately modeling real-world cellular networks and for analyzing the coverage probability and the achievable throughput. Two mathematical models, i.e., the cellular system interference model and the base station (BS) or cell distribution model, are fundamental in the coverage analysis.

A. Related Work and Motivation

The Poisson-Voronoi tesselation was proposed as early as 2001 [5]. According to [6], the interference models can generally be divided into two types: empirical models and statistical–physical models. The construction of an empirical interference model relies on first measuring the interference and then fitting a mathematical model to the data. By contrast, the derivation of a statistical–physical model usually relies on the mathematical modeling of the interference. The classic Wyner model [7] was proposed in 1994, and since then, it has been widely adopted in the analysis of cellular networks. This model assumes that the interference is constituted by the sum of the signals transmitted from the adjacent cells (typically only considering two neighbors), which is often multiplied by a fixed scaling factor or gain to represent the specific intensity of the interferers [7]–[10].

Determining the most beneficial positions of the BSs represents a critical planning problem in cellular networks. Traditional methods usually place the BSs deterministically on a regular grid, despite the fact that, in practice, the positions of BSs are influenced by many random factors. Taking into account the randomness of BS locations, in [11] and [12], a stochastic-geometry-based method for modeling the positions of the BSs was derived, whereas in [13] and [14], it was proposed that the BSs be placed according to a homogeneous Poisson point process (PPP) associated with a given intensity [13], [14]. However, since the cellular network is gradually evolving into a large-scale heterogeneous network associated with multiple-tier random BS locations, the design challenge becomes more grave. A recent contribution [15] has demonstrated that the BS locations may be drawn from a PPP, particularly for single-tier networks. In [6], the statistical–physical modeling of cochannel interference (CCI) was investigated by assuming that the geographic distribution of interferers is known *a priori* and that the interferers belong to a Poisson field, with each individual interferer having a random session life time. In [16], a mathematical theory based on a spatially homogeneous PPP was provided to analyze the effects of interference, which models the spatial distribution of the nodes over the 2-D infinite plane by PPP theory.

The PPP model was used in [13] for establishing a heterogeneous network model of a single-tier macrocell network.

Manuscript received March 5, 2014; revised August 31, 2014; accepted October 28, 2014. Date of publication October 31, 2014; date of current version September 15, 2015. This work was supported in part by the National Natural Science Foundation Project of China under Grant 61101084 and in part by the Fundamental Research Funds for the Central Universities, China. The review of this paper was coordinated by Dr. Y. Ma.

H. Zhang, L. Feng, and Y. Xie are with the Wireless Communications Laboratory, Information College, Nankai University, Tianjin 300071, China (e-mail: zhangh@nankai.edu.cn; fengliang201203@gmail.com; xyfhope@gmail.com).

S. Chen is with the School of Electronics and Computer Science, University of Southampton, Southampton SO17 1BJ, U.K., and also with King Abdulaziz University, Jeddah 21589, Saudi Arabia (e-mail: sqc@ecs.soton.ac.uk).

L. Hanzo is with School of Electronics and Computer Science, University of Southampton, Southampton SO17 1BJ, U.K. (e-mail: lh@ecs.soton.ac.uk).

Color versions of one or more of the figures in this paper are available online at http://ieeexplore.ieee.org.

Digital Object Identifier 10.1109/TVT.2014.2366597

Based on this PPP model, the calculation of the cumulative interference imposed by all surrounding BSs can be carried out with the aid of the Laplace transform and the probability generating function [13], [15]. Furthermore, the coverage probability expression was deduced for the specific scenario, when the interference experiences Rayleigh fading, and the results of [13] and [15] demonstrated that the analysis based on the PPP-aided modeling represent the lower bound of simulation results.[1] Similarly, the achievable average rate was also calculated. Although the PPP model is adopted for the analysis of cellular networks, it is only accurate for sparse networks. By contrast, it suffers from a lack of realism in the case of dense networks since it may place several BSs far too closely together, which does not make practical sense as such a situation will not occur in a real BS deployment. It may impose excessive CCI if too many BSs are deployed too densely. Noting this weakness of the PPP model, some balanced measures are suggested to alleviate this drawback in [13], but this weakness cannot be fundamentally eliminated by these measures. Moreover, the PPP-based analysis relies on the assumption that the transmitters are independently distributed [17].

A range of alternative stochastic-geometry-based methods have also been used in the analysis of wireless networks [18], [19]. For example, in [18], the Matérn hard-core process was invoked for modeling the classic carrier sense multiple access (CSMA) protocol and for analyzing its throughput, where the presence of interferers within a given radius around any transmitter was prevented. The Matérn point process [20] was modified in [19] to model the CSMA with collision avoidance, which yields more realistic results by applying the aforementioned interference-exclusion zone around all possible transmitters. However, coverage analysis based on a Matérn hard-core process is difficult to carry out [21] since the probability generating functional of a Matérn hard-core process does not exist. It was argued in [21]–[23] that only the Matérn type II process causes a level of interference comparable to that predicted by a PPP and, therefore, for interference-based performance analysis, the Matérn type II process may be safely approximated by the corresponding nonhomogeneous PPP [21]–[23].

B. Our Approach and Contributions

Against the above background, we propose a novel universal approach for tractable and accurate coverage analysis of cellular networks. Our contributions are as follows.

1) Physical Analysis of Hexagonal/Voronoi Cells: To interpret the various geometric-based cellular models from a physical perspective, we provide a tangible generic definition of the cell edge boundary for our theoretical analysis, where the cell boundary is directly linked to the path-loss exponent. Specifically, we show that the traditional hexagonal topology naturally emerges from the grid-based model, given a sufficiently high path-loss exponent, whereas the Voronoi tessellation naturally emerges from the random BS distribution model, again provided that the path-loss exponent is sufficiently high. However, such a high path-loss exponent is unrealistic in real transmission environments. Therefore, our physical analysis reveals the fundamental limitation of these purely graphic-based cellular topologies, namely, lack of the connection to the underlying signal transmission medium. In fact, we demonstrate that the cell edge boundary shows irregular near-circular shapes, given a more realistic path-loss exponent of around 3, which cannot be modeled accurately by either hexagonal or Voronoi tessellation.

2) EUDPE-Based Other-Cell Interference Model: We propose a universal model for evaluating the other-cell interference, which we refer to as the equivalent uniform-density plane-entity (EUDPE) method. This generic EUDPE model can be used to calculate the cumulative other-cell interference for all the existing BS distribution models that can be found in practice, including both stochastic and deterministic cellular network models, such as the stochastic Poisson distributed (PD) and uniformly distributed (UD) BS models and the deterministic grid-based BS model.

3) Lower Bound Analysis for Coverage Probability and Average Achievable Rate: Based on the proposed generic EUDPE interference model, we perform the low-bound analysis of both the coverage probability and the average achievable rate for various BS distribution models, specifically, the stochastic PD and UD BS models and the deterministic grid-based BS model, which may be viewed as a degenerated or special case of the UD BS model. For realistic path-loss exponents, the coverage probability and average achievable throughput results provided by our proposed analysis approach agree with the simulated coverage probability and achievable throughput. In fact, their match is as good or better than that of the PPP-based analysis. The results also show that the noise only has a modest effect on the coverage probability and achievable rate.

The remainder of this paper is organized as follows. In Section II, the downlink cellular system model is briefly introduced, which is followed by our new physical analysis of cell edge boundary. Section III is devoted to the derivation of our EUDPE-based interference model. The low-bound analysis of the coverage probability based on the EUDPE method is deduced in Section IV for both stochastic BS distribution models and deterministic grid-based BS models, whereas the corresponding low-bound analysis is presented in Section V. Our conclusions are offered in Section VI.

II. Downlink Cellular System Model

Throughout our discussions, the index set of the BSs, which are deployed according to some distribution, is denoted by Φ, whereas the serving BS's index is denoted by b_0. Furthermore, the average density of BSs is ρ. Let P be the transmitted power of a BS, R be the serving BS's coverage radius, R_{nw} be the distance from the serving BS to the edge of the network, and r_i denotes the distance from the ith BS to the user equipment (UE) concerned. If we denote the average coverage area of a BS by $\mathbb{E}[A_s]$ with $\mathbb{E}[\ ]$ representing the expectation operator, then $\mathbb{E}[A_s] = 1/\rho$. We will also use $2R$ to denote the average distance between two neighboring BSs, and we have $R \propto \sqrt{\mathbb{E}[A_s]}$.

[1] The simulation results are referred to as "experimental" or "actual" in [13], which is inappropriate.

A. SINR Model

The wireless channel linking the ith BS and the UE concerned is modeled by a complex-valued channel tap that takes into account the path loss with a path-loss exponent of α, the fast Rayleigh fading coefficient with an instantaneous power or a squared magnitude of h_i, and the channel's additive white Gaussian noise (AWGN) with noise power of σ^2. The average of the random variable h_i is denoted by $\bar{h}$; therefore, h_i follows the exponential distribution with the mean $\bar{h}$.

Let us assume that the intracell UE-to-UE interference is negligible. Then, the signal-to-interference-plus-noise ratio (SINR) experienced at this UE can be expressed as follows:

$$\text{SINR} = \frac{Ph_0 r_0^{-\alpha}}{I_r + \sigma^2} \tag{1}$$

where the interference arriving from all the interfering cells is given by

$$I_r = \sum_{i \in \Phi \setminus b_0} Ph_i r_i^{-\alpha}. \tag{2}$$

If the target SINR value is T, then the actual SINR must obey SINR $> T$, which requires

$$h_0 > P^{-1} T r_0^{\alpha} \left(\sigma^2 + I_r\right). \tag{3}$$

Thus, the probability distribution of h_0 should be taken into account in the analysis of both the coverage probability and the average rate. Furthermore, intuitively, the given SINR model determines the coverage area of each BS; therefore, it influences the cell shape or boundary.

B. Physical Analysis of Cell Edge Boundary

As aforementioned, the grid-based cellular model is convenient but is too idealistic. By contrast, the Voronoi tessellation is considered to match the random BS deployment in relative flat urban areas reasonably well [13], [24]. Hence, cellular networks can be analyzed using Voronoi diagram theory, albeit this has not been explained with the aid of a physically tangible perspective. More specifically, both the energy efficiency and coverage of cellular networks may be analyzed based on Voronoi tessellation [25], [26]. Fig. 1 shows a random distribution of the BSs with the cell boundaries corresponding to a Voronoi tessellation. Note that in both the grid-based and Voronoi-based cellular topologies, the cell boundaries are determined purely by the geometric property of the BS distribution, and they are completely independent of the actual physical interference that the network is experiencing.

To interpret the cell edge boundary from a physical perceptively, namely, linking it better to the underlying physics of signal transmission medium, let us now introduce the following definition that formally defines the cell edge boundary.

Definition 1: The cell edge boundary is constituted by the group of points where the strength of the desired signal received from the serving BS equals to the interfering signal's strength.

In other words, at the cell edge boundary, the desired signal-to-interference ratio (SIR) is equal to 1. This definition of cell edge boundary is both intuitive and practical since, within the coverage area of a BS, the desired signal should be stronger than the interfering signal, yielding SIR > 1. Let us denote the ith BS location as the point z_i, where $i \in \Phi$. Furthermore, denote the distance from z_i to a point z as $|z - z_i|$. The desired signal power at the point z provided by the ith BS is given by

$$\text{S}(z) = \mathbb{E}\left[Ph_i |z - z_i|^{-\alpha}\right] = P\bar{h}|z - z_i|^{-\alpha} \tag{4}$$

while the interfering signal's power at z is given by

$$\begin{aligned} \text{I}(z) &= \mathbb{E}\left[I_r(z)\right] = \mathbb{E}\left[\sum_{j \in \Phi \setminus i} Ph_j |z - z_j|^{-\alpha}\right] \\ &= P\bar{h} \sum_{j \in \Phi \setminus i} |z - z_j|^{-\alpha}. \end{aligned} \tag{5}$$

Thus, with respect to the ith BS, the SIR at the point z is given by

$$\text{SIR}(z) = \frac{|z - z_i|^{-\alpha}}{\sum_{j \in \Phi \setminus i} |z - z_j|^{-\alpha}}. \tag{6}$$

Therefore, at the ith cell's edge boundary, we have $\text{SIR}(z) = 1$.

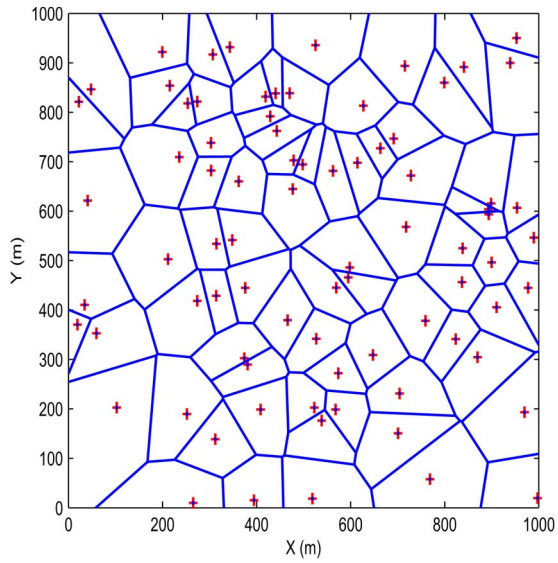

Fig. 1. Random distribution of the BSs marked by +, with the cell boundaries corresponding to a Voronoi tessellation.

In Figs. 2 and 3, the distribution of the BSs is based on the same regular grid network model, and the number of BSs is 33. As shown in Fig. 2, the shape of each cell in the network is approximately a regular circle given the path-loss exponent of $\alpha = 3$. By contrast, observe in Fig. 3 that the cell shape changes into a hexagonal one when the path-loss exponent is increased to $\alpha = 10$.

In Figs. 4 and 5, the locations of the 33 BSs are randomly drawn from the uniform distribution across the entire network area. The cells now approximately have irregularly circular shapes when the path-loss exponent is $\alpha = 3$, but interestingly, it is the Voronoi tessellation that naturally emerges when the path-loss exponent is increased to $\alpha = 10$.

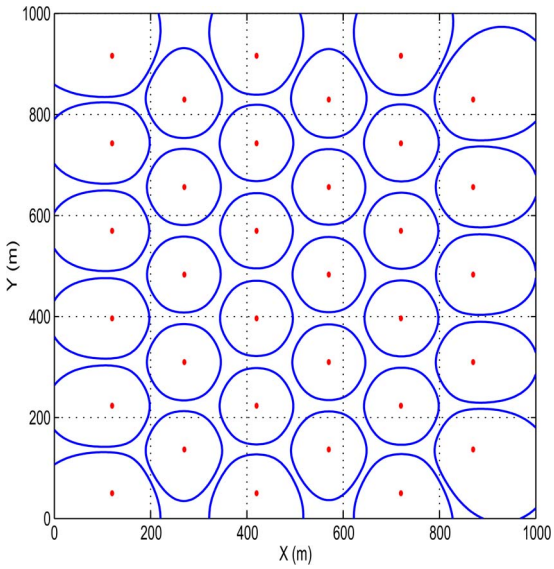

Fig. 2. Cell edge boundaries of the grid network model with the 33 BS locations marked by dots, as determined by $\mathrm{SIR}(z) = 1$. The path-loss exponent is $\alpha = 3$.

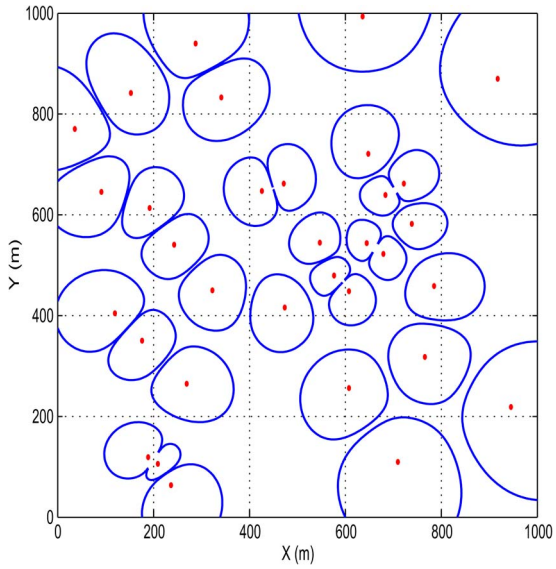

Fig. 4. Cell edge boundaries of the randomly distributed network model with the 33 BS locations marked by dots, as determined by $\mathrm{SIR}(z) = 1$. The path-loss exponent is $\alpha = 3$.

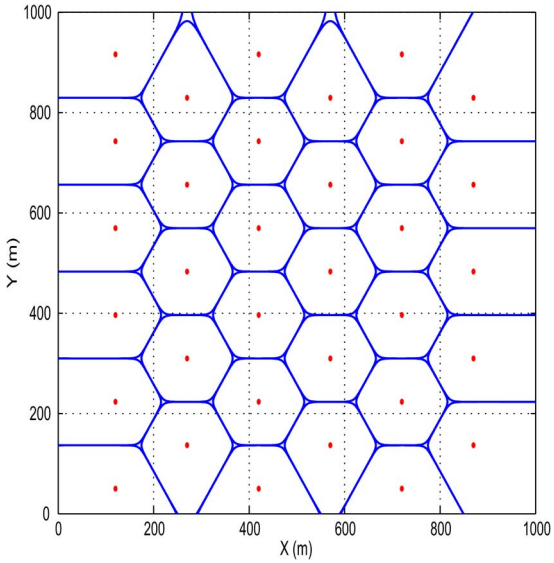

Fig. 3. Cell edge boundaries of the grid network model with the 33 BS locations marked by dots, as determined by $\mathrm{SIR}(z) = 1$. The path-loss exponent is $\alpha = 10$.

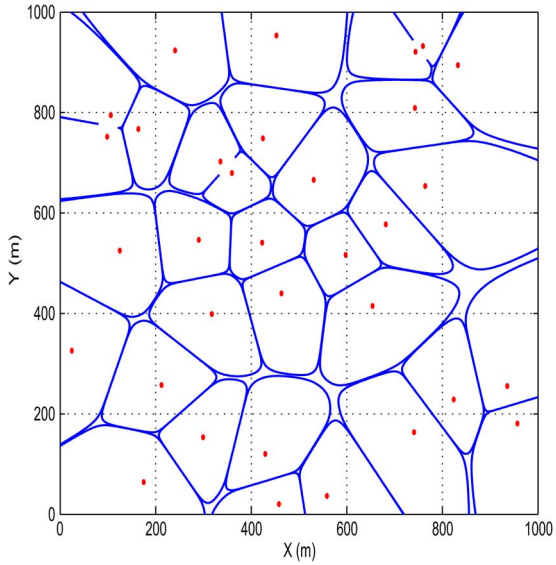

Fig. 5. Cell edge boundaries of the randomly distributed network model with the 33 BS locations marked by dots, as determined by $\mathrm{SIR}(z) = 1$. The path-loss exponent is $\alpha = 10$.

The given results demonstrate that our Definition 1 of cell edge boundary is a physically plausible one for analyzing the network, and both the hexagonal topology and the Voronoi tessellation naturally emerge according to this definition, depending on whether the geographic distribution of BSs is deterministic or random and providing that the path-loss exponent is sufficiently high. Note that such a high path-loss exponent is unrealistic in real transmission environments. Therefore, our analysis of cell edge boundary reveals a weakness of the popular hexagonal and Voronoi network topologies, namely, they do not reflect the underlying signal transmission medium. Significantly, given a more realistic path-loss exponent of approximately three, the cell edge boundary exhibits irregular near-circular cell shapes, for which neither hexagonal topology nor Voronoi tessellation can be used to accurately model. Furthermore, the "weak" coverage areas that are left outside any cell boundary, where the desired signal is weaker than the interfering signals, as shown in Fig. 4, highlight the benefits of employing collaborative relaying techniques.

III. Equivalent Uniform Density Plane-Entity for Cumulative Interference Calculation

To accurately analyze the coverage probability and the achievable rate, it is necessary to find an efficient means for

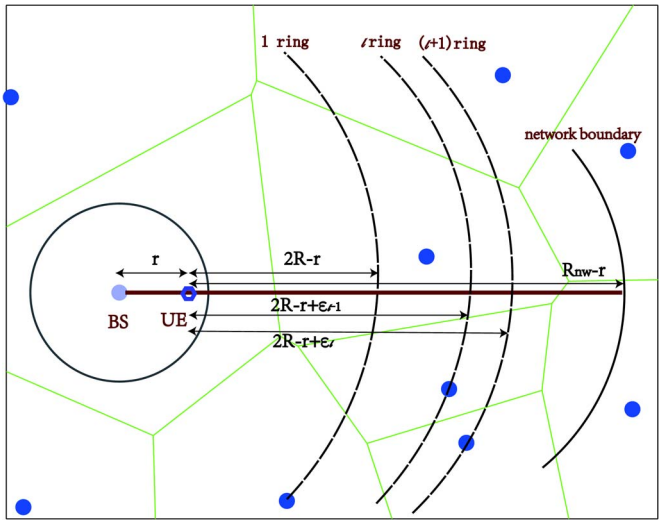

Fig. 6. Proposed EUDPE method for calculating the other-cell interference.

cumulative interference calculation. By considering the distribution of the interference imposed by the BSs in the law of large numbers and combining it with the fluid model of [27], we propose the EUDPE method for calculating the cumulative interference. The basic idea of this EDUPE method is as follows. Although the actual geographic distribution of BSs always shows a certain degree of irregularity, we may define a group of equivalent and uniformly distributed BSs for approximating the other-cell CCI. Since, in real-world cellular networks, the actual geographic distribution of BSs is often close to a uniform random distribution, such an approximation is sufficiently accurate. It is worth emphasizing however that we do not assume a uniform and random BS distribution for the actual network to be modeled. More specifically, given a network having the average BS density of ρ, we approximate this network with an equivalent network whose BSs are uniformly distributed and whose BS density is also ρ. Such a network is termed the equivalent EUDPE of the given network. With the aid of our EUDPE method, we can calculate or approximate the cumulative interference for any given network.

Fig. 6 illustrates the concept of the EUDPE, where the serving BS is assumed the origin of the polar coordinate plane. Since the coverage radius of a BS is R, the distance between two neighboring BSs is $2R$, where $R \propto (1/\sqrt{\rho})$. For notational simplification, we drop the subscript 0 from r_0 and denote the distance from the serving BS to the UE as r, where $0 \le r \le R$. Thus, the distance from the nearest interfering BS to the UE is $(2R - r)$. As shown in Fig. 6, the network's coverage area is partitioned by the N_r rings, and the distance from the UE to the lth ring is given by $(2R - r + \varepsilon_{l-1})$, where $1 \le l \le N_r$ with $\varepsilon_0 = 0$ and $(2R - r + \varepsilon_{N_r}) = R_{\rm nw} - r$. The number of BSs within the area between the lth and $(l+1)$th rings is approximately $\int_0^{2\pi} \int_{2R-r+\varepsilon_{l-1}}^{2R-r+\varepsilon_l} \rho\, z\, dz\, d\theta$ when assuming the equivalent EUDPE having the BS density of ρ. Furthermore, each of these equivalent BSs has the same instantaneous fast fading channel power of $\widetilde{h}_l$, and the mean of $\widetilde{h}_l$ is $\bar{h}$. Thus, the cumulative interference I_r can be approximated according to

$$I_r = \sum_{l=1}^{N_r} \int_0^{2\pi} \int_{2R-r+\varepsilon_{l-1}}^{2R-r+\varepsilon_l} P\widetilde{h}_l z^{-\alpha} \rho\, z\, dz\, d\theta$$
$$= \sum_{l=1}^{N_r} \frac{2\pi\rho P\widetilde{h}_l}{\alpha - 2} \left((2R - r + \varepsilon_{l-1})^{2-\alpha} - (2R - r + \varepsilon_l)^{2-\alpha}\right). \quad (7)$$

Theorem 1: The average of I_r is given by

$$\mathbb{E}[I_r] = \frac{2\pi\rho P\bar{h}}{\alpha - 2} \left((2R - r)^{2-\alpha} - (R_{\rm nw} - r)^{2-\alpha}\right). \quad (8)$$

Proof: According to the Campbell-Mecke theorem [28], we have

$$\mathbb{E}\left[\sum_{l=1}^{N_r} \frac{2\pi\rho P\widetilde{h}_l}{\alpha - 2} \left((2R - r + \varepsilon_{l-1})^{2-\alpha} - (2R - r + \varepsilon_l)^{2-\alpha}\right)\right]$$
$$= \sum_{l=1}^{N_r} \frac{2\pi\rho P\mathbb{E}[\widetilde{h}_l]}{\alpha - 2} \left((2R - r + \varepsilon_{l-1})^{2-\alpha} - (2R - r + \varepsilon_l)^{2-\alpha}\right)$$
$$= \frac{2\pi\rho P\bar{h}}{\alpha - 2} \left((2R - r)^{2-\alpha} - (R_{\rm nw} - r)^{2-\alpha}\right). \quad (9)$$

■

Typically, the path-loss exponent is $\alpha > 2$ in realistic networks. Noting that $(R_{\rm nw} - r)^{2-\alpha} \to 0$ as $R_{\rm nw} \to +\infty$, we have the following corollary.

Corollary 1: Given that the network's boundary is sufficiently far away, namely, $R_{\rm nw} \to +\infty$, we have

$$\mathbb{E}[I_r] = \frac{2\pi\rho P\bar{h}}{\alpha - 2} (2R - r)^{2-\alpha}. \quad (10)$$

IV. Coverage Probability Analysis Using Equivalent Uniform Density Plane-Entity

As mentioned earlier, the cellular system interference model and the BS geographic distribution model are required in coverage analysis. Our proposed EUDPE is a universal method for evaluating the other-cell interference for all existing BS distribution models, such as the stochastic PD and UD BS models and the deterministic grid-based model.

A. Coverage Probability Analysis Using EUDPE-PD

Since a popular geographic BS distribution is the Poisson distribution [13]–[16], we first consider the PD BS model. The probability density function (pdf) of the Poisson distribution can be derived using the method of [29]. Let λ be the intensity of the Poisson distribution that models the BS geographic distribution and R be the average coverage radius of a cell. Then, the probability of having no BS that is closer than x is given by

$$\mathbb{P}\{r > x\} = \mathbb{P}\{\text{No BS closer than } x\} = e^{-\lambda\pi x^2}. \quad (11)$$

The corresponding cumulative distribution function (cdf) is then given by

$$\mathbb{P}\{r \le x\} = F(x) = 1 - e^{-\lambda\pi x^2}. \tag{12}$$

Therefore, the pdf is defined as

$$f(r) = \frac{d\,F(r)}{d\,r} = 2\pi\lambda\, r\, e^{-\pi\lambda r^2}. \tag{13}$$

Given the SINR threshold T, the intensity λ and the path-loss exponent α, the coverage probability is defined as

$$\begin{aligned} p_c(T,\lambda,\alpha) &= \mathbb{E}_r\left[\mathbb{E}_{I_r}\left[\mathbb{P}\{\text{SINR} > T\}\right]\right] \\ &= \int_{r>0} \mathbb{E}_{I_r}\left[\mathbb{P}\left\{h_0 > P^{-1}Tr^{\alpha}(\sigma^2 + I_r)\right\}\right] 2\pi\lambda r e^{-\pi\lambda r^2}\, dr \end{aligned} \tag{14}$$

where $\mathbb{E}_r[\bullet]$ denotes the expectation with respect to the random variable r.

1) Lower Bound for the Probability of SINR Larger Than Threshold: Noting that h_0 obeys the exponential distribution with the mean $\bar{h}$, the probability of the SINR larger than the threshold T (averaged over the interference) is given by

$$\begin{aligned} &\mathbb{E}_{I_r}\left[\mathbb{P}\left\{h_0 > P^{-1}Tr^{\alpha}(\sigma^2 + I_r)\right\}\right] \\ &\qquad = e^{-\bar{h}P^{-1}Tr^{\alpha}\sigma^2}\mathbb{E}_{I_r}\left[e^{-\bar{h}P^{-1}Tr^{\alpha}I_r}\right]. \end{aligned} \tag{15}$$

Theorem 2: A lower bound for the probability of the SINR greater than the threshold T is expressed as

$$\mathbb{E}_{I_r}\left[\mathbb{P}\left\{h_0 > P^{-1}Tr^{\alpha}(\sigma^2 + I_r)\right\}\right] \ge e^{-\bar{h}Tr^{\alpha}\eta(\alpha,r)} \tag{16}$$

where

$$\eta\,(\alpha, r) = P^{-1}\sigma^2 + \frac{2\pi\rho\bar{h}}{\alpha - 2}\left((2R - r)^{2-\alpha} - (R_{\text{nw}} - r)^{2-\alpha}\right). \tag{17}$$

Proof: According to Jensen's inequality [30], we have

$$\mathbb{E}_{I_r}\left[e^{-\bar{h}P^{-1}Tr^{\alpha}I_r}\right] \ge e^{-\bar{h}P^{-1}Tr^{\alpha}\mathbb{E}[I_r]}. \tag{18}$$

Substituting (18) into (15) and noting $\mathbb{E}[I_r]$ of (8) leads to (16) with $\eta(\alpha, r)$ given in (17). ■

Corollary 2: Given that the network boundary is sufficiently far away, namely, $R_{\text{nw}} \to +\infty$

$$\mathbb{E}_{I_r}\left[\mathbb{P}\left\{h_0 > P^{-1}Tr^{\alpha}(\sigma^2 + I_r)\right\}\right] \ge e^{-\bar{h}Tr^{\alpha}\xi(\alpha,r)} \tag{19}$$

where

$$\xi(\alpha, r) = P^{-1}\sigma^2 + \frac{2\pi\rho\bar{h}}{\alpha - 2}(2R - r)^{2-\alpha}. \tag{20}$$

2) Lower Bound for the Coverage Probability: A lower bound for the coverage probability $p_c(T, \lambda, \alpha)$ is given by the following theorem.

Theorem 3: For the network where the BS geographic distribution obeys the Poisson distribution of intensity λ, a lower bound for the coverage probability $p_c(T, \lambda, \alpha)$ is given by

$$p_{cl}(T, \lambda, \alpha) = \pi\lambda \int_0^{R^2} e^{-\bar{h}Tv^{\alpha/2}\psi(\alpha,v) - \pi\lambda v}\, dv \tag{21}$$

where R is the coverage radius of the serving BS, and

$$\begin{aligned} \psi(\alpha, v) = P^{-1}\sigma^2 + \frac{2\pi\rho\bar{h}}{\alpha - 2}\Big((2R - v^{1/2})^{2-\alpha} \\ - (R_{\text{nw}} - v^{1/2})^{2-\alpha}\Big). \end{aligned} \tag{22}$$

Proof: From (14) and Theorem 2, as well as noting that $r \le R$, we have

$$p_{cl}(T, \lambda, \alpha) = \int_0^{R} 2\pi\lambda r e^{-\bar{h}Tr^{\alpha}\eta(\alpha,r) - \pi\lambda r^2}\, dr. \tag{23}$$

By defining $r^2 = v$, (23) is transformed into (21) with $\psi(\alpha, v)$ given in (22). ■

Corollary 3: Given that the network boundary is sufficiently far away, namely, $R_{\text{nw}} \to +\infty$, a lower bound for the coverage probability $p_c(T, \lambda, \alpha)$ is expressed as

$$p_{cl}(T, \lambda, \alpha) = \pi\lambda \int_0^{R^2} e^{-\bar{h}Tv^{\alpha/2}\chi(\alpha,v) - \pi\lambda v}\, dv \tag{24}$$

where

$$\chi(\alpha, v) = P^{-1}\sigma^2 + \frac{2\pi\rho\bar{h}}{\alpha - 2}(2R - v^{1/2})^{2-\alpha}. \tag{25}$$

Remark 1: In the coverage analysis for the EUDPE-PD model, the average coverage radius R is related to the average cell area $\mathbb{E}[A_s]$. Noting $R \propto \sqrt{\mathbb{E}[A_s]}$ and $\mathbb{E}[A_s] = 1/\rho$, we may use

$$R = \frac{c_f}{\sqrt{\rho}} \tag{26}$$

where c_f is an empirically chosen factor. For example, if the average cell is defined by a square shape, we have $\mathbb{E}[A_s] = 4R^2$; therefore, we have $c_f = 1/2 = 0.5$. On the other hand, if the average coverage area is calculated according to a hexagonal one, we have $\mathbb{E}[A_s] = 2\sqrt{3}R^2$, yielding $c_f = 1/\sqrt{2\sqrt{3}} \approx 0.54$, whereas for the average circle-shape cell, we have $c_f = 1/\sqrt{\pi} \approx 0.56$.

B. Coverage Probability Analysis Using EUDPE-UD

For many practical cellular networks, the geographic BS distribution is often close to a uniform random distribution. Therefore, we next consider the UD BS model with the average

density of BSs given by ρ. In this case, the corresponding cdf is given by

$$\mathbb{P}\{z \le x\} = F(x) = \frac{x^2}{c_{\rm nm}^2}\rho, \quad 0 \le x \le R \tag{27}$$

where $c_{\rm nm}^2$ is a normalization factor, and R is the coverage radius of the serving BS. Thus, the pdf is given as

$$f(r) = \frac{2\rho}{c_{\rm nm}^2} r, \quad 0 \le r \le R. \tag{28}$$

The normalization factor $c_{\rm nm}^2$ is determined as follows. Assume that $E[A_s] = R^2/c_f^2$, where c_f is defined in (26), and further note that $E[A_s] = 1/\rho$. From $\int_0^R f(r)\,dr = 1$, we obtain $c_{\rm nm}^2 = c_f^2$.

The coverage probability is therefore defined as

$$\begin{aligned} p_c(T,\rho,\alpha) &= \mathbb{E}_r\left[\mathbb{E}_{I_r}\left[\mathbb{P}\{\text{SINR} > T\}\right]\right] \\ &= \frac{\rho}{c_f^2}\int_0^R \mathbb{E}_{I_r}\left[\mathbb{P}\left\{h_0 > P^{-1}Tr^{\alpha}(\sigma^2 + I_r)\right\}\right] 2r\,dr. \end{aligned} \tag{29}$$

A lower bound of $\mathbb{E}_{I_r}[\mathbb{P}\{h_0 > P^{-1}Tr^{\alpha}(\sigma^2 + I_r)\}]$ is given in Theorem 2. Similar to the case of the EUDPE-PD expressed in Theorem 3, therefore, a lower bound for the coverage probability $p_c(T,\rho,\alpha)$ is given by the following theorem.

Theorem 4: For the network where the BS geographic distribution obeys the uniform random distribution with an average BS density of ρ, a lower bound for the coverage probability $p_c(T,\rho,\alpha)$ is given by

$$p_{cl}(T,\rho,\alpha) = \frac{\rho}{c_f^2}\int_0^{R^2} e^{-\bar{h}Tv^{\alpha/2}\psi(\alpha,v)}\,dv \tag{30}$$

where $\psi(\alpha,v)$ is defined in (22).

Corollary 4: Given that the network boundary is sufficiently far away, a lower bound for the coverage probability $p_c(T,\rho,\alpha)$ is expressed by

$$p_{cl}(T,\rho,\alpha) = \frac{\rho}{c_f^2}\int_0^{R^2} e^{-\bar{h}Tv^{\alpha/2}\chi(\alpha,v)}\,dv \tag{31}$$

where $\chi(\alpha,v)$ is defined in (25).

Remark 2: How to set the average coverage radius R is explained in Remark 1. Specifically, we may use $R = c_f/\sqrt{\rho}$, where c_f is an empirically chosen factor.

C. Coverage Probability Analysis Using EUDPE-Grid

With the aid of the EUDPE method, it is straightforward to carry out the coverage probability analysis for all the traditional deterministic grid-based cellular network models, such as the squared and hexagonal ones. This is because the coverage probability analysis using the EUDPE-Grid model is simply a degenerated or special case of the EUDPE-UD-based analysis, where the density of BSs ρ is identical everywhere in the network, and every cell has the identical shape with the same area A_s. Therefore, the lower bounds of the coverage probability for the finite-size and infinite-size grid-based network models are given in Theorem 4 and Corollary 4, respectively. Moreover, choosing $R = 1/(2\sqrt{\rho})$ corresponds to the grid-based network with squared cells, whereas using $R = 1/(\sqrt{2\sqrt{3}}\sqrt{\rho})$ is related to considering the grid-based network with hexagonal cells. In general, we may use $R = c_f/\sqrt{\rho}$ for any deterministic grid-based network by choosing an appropriate value for c_f. It becomes obvious that, under the equivalent network environment of the same ρ and R values, the coverage probability obtained by the EUDPE-Grid-based analysis is identical to that obtained by the EUDPE-UD-based analysis.

D. Numerical Results for Coverage Probability

We evaluated the coverage probability first by simulation and used the simulated results as the benchmark for the comparison with our theoretical analytic results. We considered two scenarios. The first case is a single-tier network constructed by macrocells, obeying the uniform random BS distribution and the cellular channel model described in Section II, whereas the second network followed a Poisson BS distribution and obeyed the same cellular channel model of Section II. Given the SINR threshold T, the path-loss exponent α, and the SINR value, the simulated coverage probability was calculated using the pseudocodes presented in Algorithm 1. In the simulation, we set the number of BSs to $N_{\rm BS} = 80$, the number of UEs to $N_{\rm UE} = 10\,000$, the network coverage area to Network Area $= 1000 \times 1000$ m^2, and the number of sample simulations to $N_{\max} = 100$. The average density of BSs was then given as

$$\rho = \frac{N_{\rm BS}}{\text{Network Area}}[\text{BSs/m}^2]. \tag{32}$$

For the Poisson distribution, its intensity was $\lambda = \rho$. We compared our low-bound coverage probability results based on the EUDPE-PD and EUDPE-UD models with that of the PPP-based analysis [13]. Since the PPP method can only consider the case of an infinitely large network, we assumed the network boundary $R_{\rm nw} \to +\infty$. In the following comparison, the simulation results obtained by the network with the uniform random BS distribution are labeled as Simulated data 1, whereas the simulation results yielded by the network with the Poisson BS distribution are denoted Simulated data 2.

Algorithm 1 Network Simulation to Evaluate the Coverage Probability.

1: Give the number of BSs $N_{\rm BS}$, the Network Area, and the number of UEs $N_{\rm UE}$;
2: Give the maximum number of sample simulations $N_{\max}$;
3: Set Average Coverage Probability $= 0$;
4: **for** $N_{\rm sm} = 1$ to $N_{\max}$ **do**
5: Uniformly and randomly draw the $N_{\rm BS}$ BSs over Network Area, or draw the $N_{\rm BS}$ BSs over Network Area by the Poisson distribution;

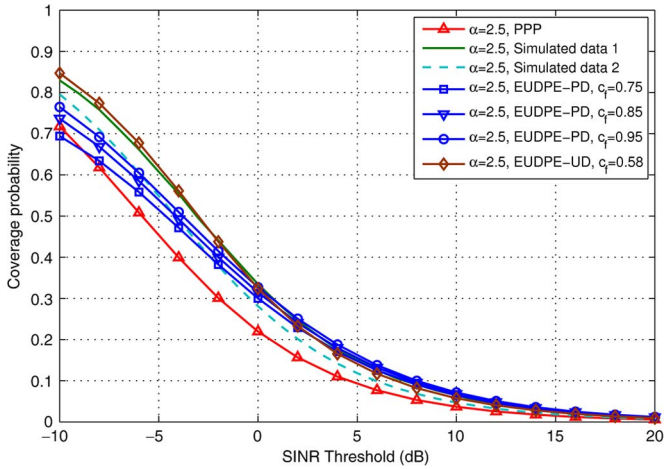

Fig. 7. Comparison of the coverage probabilities based on three different models to the network simulation results, given the path-loss exponent of $\alpha = 2.5$ and no noise, i.e., the AWGN power $\sigma^2 = 0$ and SINR = SIR.

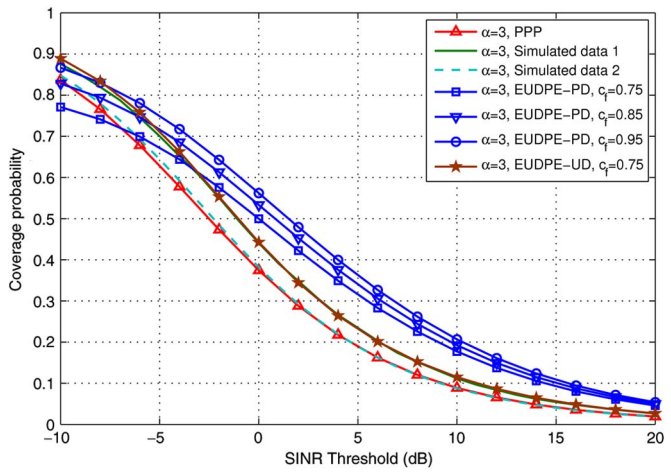

Fig. 8. Comparison of the coverage probabilities based on three different models to the network simulation results, given the path-loss exponent of $\alpha = 3$ and no noise, i.e., the AWGN power $\sigma^2 = 0$ and SINR = SIR.

6: Uniformly and randomly draw the N_{UE} UEs over Network Area;
7: Initialization: count $= 0$;
8: **for** $j = 1$ to N_{UE}, **do**
9: **if** $\mathrm{SINR}_j \geq T$ **then**
10: count $=$ count $+ 1$;
11: **end if**
12: **end for**
13: Coverage Probability $=$ count$/N_{\mathrm{UE}}$;
14: Average Coverage Probability $+ =$ Coverage Probability;
15: **end for**
16: Average Coverage Probability $/ = N_{\max}$.

Given the path-loss exponent of $\alpha = 2.5$ and assuming no AWGN or $\sigma^2 = 0$, which implies SINR = SIR, Fig. 7 shows the coverage probabilities calculated based on the three analytic models, in comparison to the coverage probabilities obtained by the two different network simulations, when varying the SINR threshold. It is shown in Fig. 7 that the coverage probability analysis results of our proposed EUDPE-PD and EUDPE-UD models agree with both simulation results well, better than the PPP-based analysis. When the path-loss exponent is increased to $\alpha = 3$ and 4, the results obtained are shown in Figs. 8 and 9, respectively, where it can be seen that the EUDPE-UD analysis agrees with the simulation result based on the network with the uniform random BS distribution better than the other two models, whereas the PPP-based analysis agrees better with the simulation result of the network with the Poisson BS distribution better than the other two models.

It is worth emphasizing that because there exist no real network performance data to validate an analysis model, we can only rely on the simulated data. When we have an analysis model agrees with a particular simulation result better than another analysis model, it does not imply that the former is better than the latter. The particular simulation result may not actually represent the true real network performance and, moreover, the simulation conditions may not actually match those imposed on an analysis model. What we can claim however is that, if

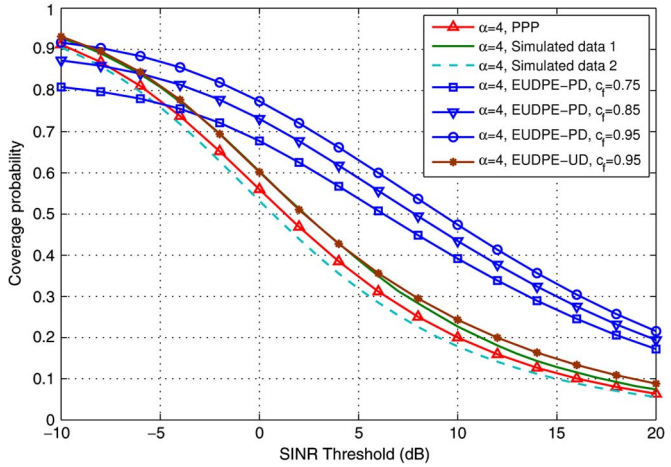

Fig. 9. Comparison of the coverage probabilities based on three different models to the network simulation results, given the path-loss exponent of $\alpha = 4$ and no noise, i.e., the AWGN power $\sigma^2 = 0$ and SINR = SIR.

an analysis model agrees well with simulation data, it is a reasonable tool for network analysis and planning. Similarly, if a lower bound coverage probability derived by an analysis model appears to be larger than a simulated coverage probability, it does not imply that this analysis model is wrong. Again, the simulation conditions may not actually match those imposed on the analysis model. For example, we assumed that the network boundary $R_{\mathrm{nw}} \to +\infty$ for the proposed EUDPE-PD and EUDPE-UD models and the PPP-based analysis for the fair comparison of the three analysis models since the PPP method can only be applied for the case of an infinitely large network. However, the simulated network size was 1000×1000 m^2 and not infinitely large. As shown earlier, another advantage of our analysis approach over the PPP-based method is that our method can be applied to analyze finite-size networks.

In our EUDPE-based analysis, the empirical chosen factor c_f is related to the average cell shape and size. The theoretical explanations of this area factor c_f are given in Remark 1. Observe from Fig. 7 that, for the path-loss exponent $\alpha = 2.5$, an appropriate value of this area factor for our EUDPE-UD model is $c_f = 0.58$, which is, in fact, close to the case of the average

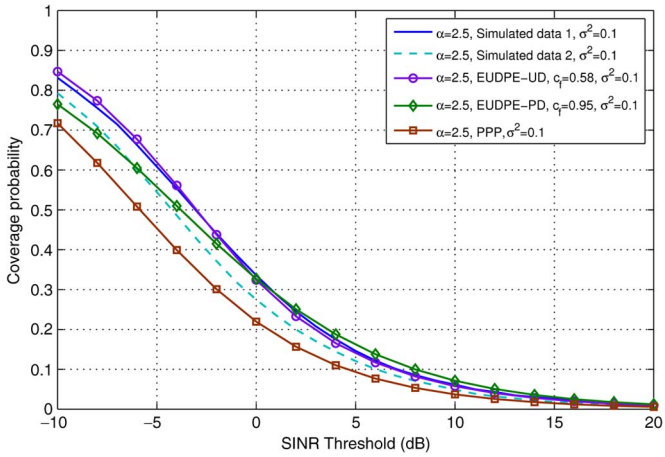

Fig. 10. Comparison of the coverage probabilities based on three different models to the network simulation results, given the path-loss exponent of $\alpha = 2.5$ and the AWGN power $\sigma^2 = 0.1$.

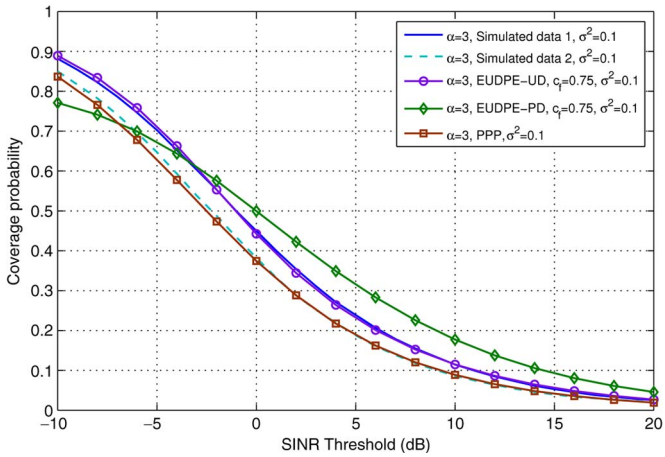

Fig. 11. Comparison of the coverage probabilities based on three different models to the network simulation results, given the path-loss exponent of $\alpha = 3$ and the AWGN power $\sigma^2 = 0.1$.

circle-shaped cell. However, as shown in Figs. 8 and 9, as α increases, the appropriate area factor c_f value also increases. A plausible explanation for this phenomenon is offered as follows. As the path-loss exponent α increases, the effective coverage area R^2/c_f^2 of the serving BS is reduced, and this corresponds to an increase in the area factor c_f.

Next, the effect of noise imposed on the achievable coverage probability was investigated by setting the AWGN power to $\sigma^2 = 0.1$ or $10\log_{10}(1/\sigma^2) = 10$ dB, and the results obtained are given in Figs. 10–12, respectively, for the three different values of α. For graphic clarity, we only draw a single EUDPE-PD-based coverage probability associated with an appropriate area factor c_f value in each of these three figures. Again, the same observations as those drawn for Figs. 7–9 can be made, namely, for the case of $\alpha = 2.5$, the EUDPE-UD-based analysis agrees with the both simulation results better than the PPP-based analysis, whereas for higher α values, the EUDPE-UD analysis matches better with the simulated results based on the uniform random BS distribution, and the PPP-based analysis agrees better with the simulated results based

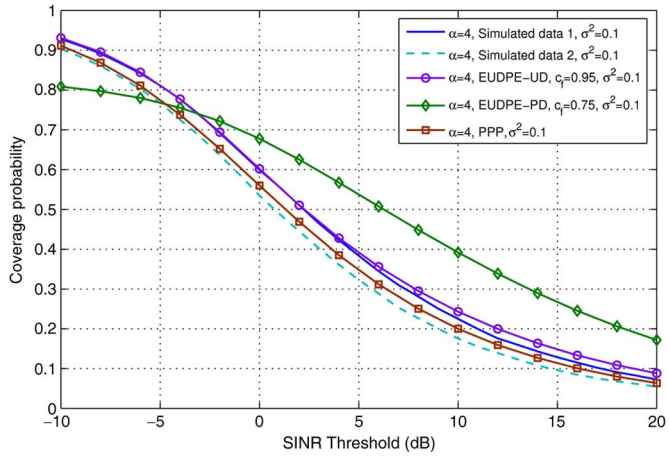

Fig. 12. Comparison of the coverage probabilities based on three different models to the network simulation results, given the path-loss exponent of $\alpha = 4$ and the AWGN power $\sigma^2 = 0.1$.

on the Poisson BS distribution. Upon comparing Figs. 10–12 with Figs. 7–9, it can be seen that the effect of the channel AWGN to the achievable coverage probability is minor. For example, observe that the simulated-data-2 curve in Fig. 7 almost matches the simulated-data-2 curve in Fig. 10, whereas the PPP-analysis-based curve in Fig. 7 is almost identical to the PPP-analysis-based curve in Fig. 10. Similarly, the other three coverage probability curves in Fig. 10 also closely match the corresponding coverage probability curves in Fig. 7.

V. Average Achievable Rate Analysis Using Equivalent Uniform Density Plane-Entity

Let us now apply the proposed EUDPE method to analyze the average achievable throughput. According to Shannon's theory, under the idealized simplifying condition of having a Gaussian interference owing to the central limit theorem, the average achievable rate is defined as [12]

$$C \triangleq \mathbb{E}\left[\ln\left(1 + \mathrm{SINR}\right)\right]. \tag{33}$$

Since we are concerned with the system's achievable throughput, we will consider the case of the network boundary being sufficiently far away, i.e., $R_{\mathrm{nw}} \to +\infty$.

A. Average Achievable Rate Analysis Using EUDPE-PD

Again, we first consider the case that the geographic BS distribution follows a Poisson distribution, and we have the following result.

Theorem 5: For the network where the BS geographic distribution obeys the Poisson distribution of intensity λ, a lower bound for the average achievable throughput is given by

$$C_l(\lambda,\alpha) = \pi\lambda \int_0^{R^2} e^{-\pi\lambda v} \left(\int_{t>0} e^{-\bar{h} v^{\alpha/2}(e^t-1)\chi(\alpha,v)}\, dt \right) dv \tag{34}$$

where $\chi(\alpha, v)$ is given in (25).

Proof: According to [12], we have

$$C(\lambda,\alpha)=\int_0^R 2\pi\lambda r e^{-\pi\lambda r^2} \times \int_{t>0}\mathbb{E}_{I_r}\left[\mathbb{P}\left\{h_0>P^{-1}r^{\alpha}(e^t-1)(\sigma^2+I_r)\right\}\right]dt\,dr. \quad (35)$$

Similar to Corollary 2, we have

$$\mathbb{E}_{I_r}\left[\mathbb{P}\left\{h_0>P^{-1}r^{\alpha}(e^t-1)(\sigma^2+I_r)\right\}\right] \geq e^{-\bar{h}r^{\alpha}(e^t-1)\xi(\alpha,r)} \quad (36)$$

where $\xi(\alpha,r)$ is defined in (20). Thus, a lower bound of $C(\lambda,\alpha)$ is given by

$$C_l(\lambda,\alpha)=\int_0^R 2\pi\lambda r e^{-\pi\lambda r^2}\left(\int_{t>0} e^{-\bar{h}r^{\alpha}(e^t-1)\xi(\alpha,r)}\,dt\right)dr. \quad (37)$$

By defining $v=r^2$ in (37), we obtain (34). ■

Corollary 5: In the noise-free case, namely, $\sigma^2=0$, a lower bound for the average achievable throughput is

$$C_l(\lambda,\alpha)=\pi\lambda\int_0^{R^2} e^{-\pi\lambda v}\left(\int_{t>0} e^{-\bar{h}v^{\alpha/2}(e^t-1)\bar{\chi}(\alpha,v)}\,dt\right)dv \quad (38)$$

where

$$\bar{\chi}(\alpha,v)=\frac{2\pi\rho\bar{h}}{\alpha-2}(2R-v^{1/2})^{2-\alpha}. \quad (39)$$

B. Average Achievable Rate Analysis Using EUDPE-UD

Next, we consider the case that the geographic BS distribution follows a uniform random distribution, and we have the following result.

Theorem 6: For the network where the BS geographic distribution obeys the uniform random distribution with an average BS density of ρ, a lower bound for the average achievable throughput is given by

$$C_l(\rho,\alpha)=\frac{\rho}{c_f^2}\int_0^{R^2}\left(\int_{t>0} e^{-\bar{h}v^{\alpha/2}(e^t-1)\chi(\alpha,v)}dt\right)dv \quad (40)$$

where $\chi(\alpha,v)$ is given in (25).

Proof: Noting that the average achievable throughput is defined as

$$C(\lambda,\alpha)=\frac{\rho}{c_f^2}\int_0^R 2r \times\int_{t>0}\mathbb{E}_{I_r}\left[\mathbb{P}\left\{h_0>P^{-1}r^{\alpha}(e^t-1)(\sigma^2+I_r)\right\}\right]dt\,dr \quad (41)$$

the proofs are similar to the proofs for Theorem 5. ■

Corollary 6: In the noise-free case, namely, $\sigma^2=0$, a lower bound for the average achievable throughput is

$$C_l(\rho,\alpha)=\frac{\rho}{c_f^2}\int_0^{R^2}\left(\int_{t>0} e^{-\bar{h}v^{\alpha/2}(e^t-1)\bar{\chi}(\alpha,v)}\,dt\right)dv. \quad (42)$$

where $\bar{\chi}(\alpha,v)$ is given in (39).

Remark 3: It is straightforward to carry out the average achievable throughput analysis for any deterministic grid-based cellular network model, because the EUDPE-Grid model is a special case of the EUDPE-UD model. Therefore, the lower bound of the average achievable throughput for the grid-based network model is also given in Theorem 6. Moreover, under the equivalent network environment of the same ρ and R values, the lower bound of the average achievable throughput obtained by the EUDPE-Grid-based analysis is identical to that obtained by the EUDPE-UD-based analysis.

C. Numerical Results for Average Achievable Rate

Assuming a unity frequency reuse factor, we compare the lower bounds of the average achievable throughput obtained by the proposed EUDPE-PD- and EUDPE-UD-based analyses to that of the PPP-based analysis [12] in Fig. 13 by varying the path-loss exponent value. The simulated average achievable throughputs obtained from the two network simulations with the uniform random BS distribution and the Poisson BS distribution are labeled as Simulated rate 1 and Simulated rate 2, respectively, and they are also given in Fig. 13 as the benchmark. For our proposed EUDPE-PD and EUDPE-UD-based analysis and the network simulations, both the noise-free and noisy results are presented. However, for the PPP-based average achievable throughput analysis, only the noise-free case is provided in [12]; therefore, in Fig. 13, we only present the noise-free PPP-based result. It can be observed that all the three theoretical analysis based results and the simulation data all reveal that the average achievable throughput increases linearly, as the path-loss exponent increases. More specifically, all the analytical and simulated data have accurate linear fitting. It is also shown in Fig. 13 that our proposed EUDPE-PD- and EUDPE-UD-based analyses agree with the two simulated results better than the PPP-based analysis, particularly for the path-loss exponent $\alpha\leq 4.5$. The results of Fig. 13 also show that the noise only has a minor effect on the average achievable throughput, which is expected as we consider the interference-limited scenario with a unity frequency reuse factor.

VI. Conclusion

We have proposed a universal approach for accurately analyzing the coverage probability and average achievable throughput of cellular networks. More specifically, we have derived a generic EUDPE procedure for evaluating the other-cell interference. Based on this EUDPE interference model, we have derived the lower bounds of both the coverage probability and average achievable throughput for various practical BS distribution models, including the stochastic Poisson distributed

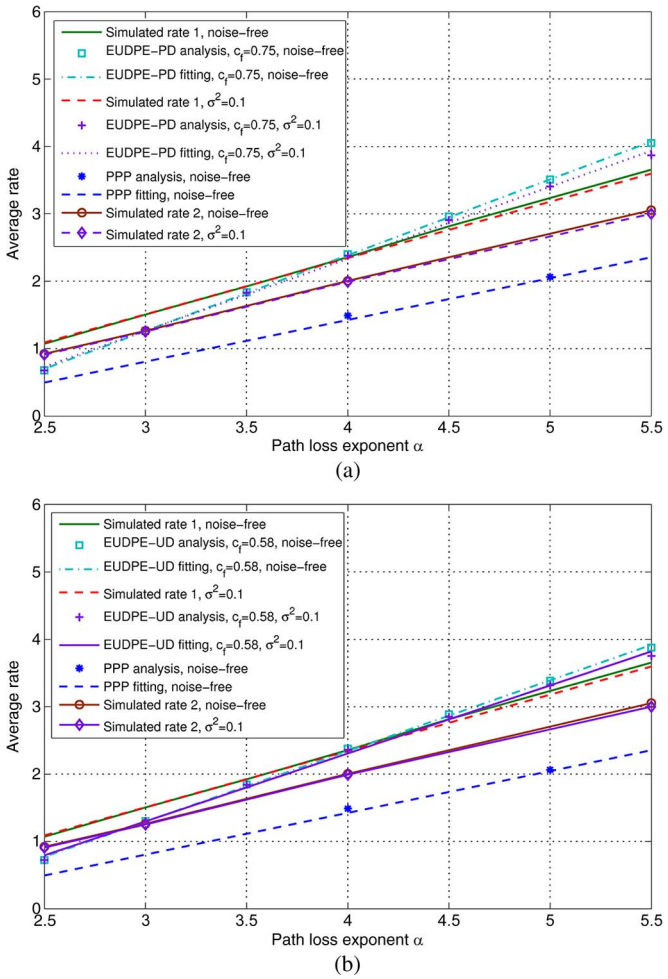

Fig. 13. Comparison of the average achievable throughputs based on three different models to the network simulation results, given different path-loss exponent values. (a) EUDPE-PD and PPP models and (b) EUDPE-UD and PPP models.

model, uniformly and randomly distributed model, and the deterministic grid-based model. Extensive simulation results have validated that the coverage probability and average throughput obtained by our proposed universal analysis method agree with the simulated coverage probability and average throughput at least as closely as those obtained by the popular existing PPP-based analysis, if not better. In addition, we have also introduced a generic and physical definition of cell edge boundary. We have shown that the popular hexagonal and Voronoi network topologies only emerge from the grid-based network model and the random BS distribution model, respectively, given an unrealistic high path-loss exponent according to this definition. Moreover, we have demonstrated that the cell edge boundary shows irregular near-circular shapes, given a more realistic path-loss exponent, which cannot be modeled accurately by either hexagonal or Voronoi topology.

REFERENCES

[1] A. Damnjanovic *et al.*, "A survey on 3GPP heterogeneous networks," *IEEE Wireless Commun.*, vol. 18, no. 3, pp. 10–21, Jun. 2011.

[2] J. G. Andrews, "Seven ways that hetnets are a cellular paradigm shift," *IEEE Commun. Mag.*, vol. 51, no. 3, pp. 136–144, Mar. 2013.

[3] A. Ghosh, *et al.*, "Heterogeneous cellular networks: From theory to practice," *IEEE Commun. Mag.*, vol. 50, no. 6, pp. 54–64, Jun. 2012.

[4] J. G. Andrews, H. Claussen, M. Dohler, S. Rangan, and M. C. Reed, "Femtocells: Past, present, and future," *IEEE J. Sel. Areas Commun.*, vol. 30, no. 3, pp. 497–508, Apr. 2012.

[5] F. Baccelli and B. Błaszczyszyn, "On a coverage process ranging from the Boolean model to the Poisson Voronoi tessellation, with applications to wireless communications," *Adv. Appl. Probab. (SGSA)*, vol. 33, pp. 293–323, 2001.

[6] X. Yang and A. P. Petropulu, "Co-channel interference modeling and analysis in a Poisson field of interferers in wireless communications," *IEEE Trans. Signal Process.*, vol. 51, no. 1, pp. 64–76, Jan. 2003.

[7] A. D. Wyner, "Shannon-theoretic approach to a Gaussian cellular multiple-access channel," *IEEE Trans. Inf. Theory*, vol. 40, no. 6, pp. 1713–1727, Nov. 1994.

[8] S. Shamai and A. D. Wyner, "Information-theoretic considerations for symmetric, cellular, multiple-access fading channels, Part I," *IEEE Trans. Inf. Theory*, vol. 43, no. 6, pp. 1877–1894, Nov. 1997.

[9] S. Shamai and A. D. Wyner, "Information-theoretic considerations for symmetric, cellular, multiple-access fading channels, Part II," *IEEE Trans. Inf. Theory*, vol. 43, no. 6, pp. 1895–1911, Nov. 1997.

[10] J. Xu, J. Zhang, and J. G. Andrews, "On the accuracy of the Wyner model in cellular networks," *IEEE Trans. Wireless Commun.*, vol. 10, no. 9, pp. 3098–3109, Sep. 2011.

[11] F. Baccelli, M. Klein, M. Lebourges, and S. Zuyev, "Stochastic geometry and architecture of communication networks," *Telecommun. Syst.*, vol. 7, no. 1–3, pp. 209–227, Jun. 1997.

[12] T. X. Brown, "Cellular performance bounds via shotgun cellular systems," *IEEE J. Sel. Areas Commun.*, vol. 18, no. 11, pp. 2443–2455, Nov. 2000.

[13] J. G. Andrews, F. Baccelli, and R. K. Ganti, "A tractable approach to coverage and rate in cellular networks," *IEEE Trans. Commun.*, vol. 59, no. 11, pp. 3122–3134, Nov. 2011.

[14] R. W. Heath and M. Kountouris, "Modeling heterogeneous network interference," in *Proc. IEEE ITA*, San Diego, CA, USA, Feb. 5–10, 2012, pp. 17–22.

[15] H. S. Dhillon, R. K. Ganti, F. Baccelli, and J. G. Andrews, "Modeling and analysis of K-tier downlink heterogeneous cellular networks," *IEEE J. Sel. Areas Commun.*, vol. 30, no. 3, pp. 550–560, Apr. 2012.

[16] M. Z. Win, P. C. Pinto, and L. A. Shepp, "A mathematical theory of network interference and its applications," *Proc. IEEE*, vol. 97, no. 2, pp. 205–230, Feb. 2009.

[17] A. Busson and G. Chelius, "Point processes for interference modeling in CSMA/CA ad-hoc networks," in *Proc. 6th ACM Symp. Performance Eval. Wireless Ad Hoc, Sens., Ubiquitous Netw.*, Tenerife, Canary Islands, Spain, Oct. 26–30, 2009, pp. 33–40.

[18] F. Baccelli, B. Błaszczyszyn, and P. Mühlethaler, "An Aloha protocol for multihop mobile wireless networks," *IEEE Trans. Inf. Theory*, vol. 52, no. 2, pp. 421–436, Feb. 2006

[19] H. Q. Nguyen, F. Baccelli, and D. Kofman, "A stochastic geometry analysis of dense IEEE 802.11 networks," in *Proc. 26th IEEE INFOCOM*, Anchorage, AK, USA, May 6–12, 2007, pp. 1199–1207.

[20] M. L. Huber and R. L. Wolpert, "Likelihood-based inference for Matérn type-III repulsive point processes," *Adv. Appl. Probab.*, vol. 41, no. 4, pp. 958–977, Dec. 2009.

[21] M. Haenggi, "Mean interference in hard-core wireless networks," *IEEE Commun. Lett.*, vol. 15, no. 8, pp. 792–794, Aug. 2011.

[22] A. Hasan and J. G. Andrews, "The guard zone in wireless ad hoc networks," *IEEE Trans. Wireless Commun.*, vol. 6, no. 3, pp. 897–906, Mar. 2007.

[23] B. Cho, K. Koufos, and R. Jantti, "Bounding the mean interference in Matérn type II hard-core wireless networks," *IEEE Wireless Commun. Lett.*, vol. 2, no. 5, pp. 563–566, Oct. 2013.

[24] F. Jarai-Szabo and Z. Neda, "On the size-distribution of Poisson Voronoi cells," *Phys. A, Statist. Mech. Appl.*, vol. 385, no. 2, pp. 518–526, Feb. 2007.

[25] D. Cao, S. Zhou, and Z. Niu, "Optimal combination of base station densities for energy-efficient two-tier heterogeneous cellular networks," *IEEE Trans. Wireless Commun.*, vol. 12, no. 9, pp. 4350–4362, Sep. 2013.

[26] S. Lee and K. Huang, "Coverage and economy of cellular networks with many base stations," *IEEE Commun. Lett.*, vol. 16, no. 7, pp. 1038–1040, Jul. 2012.

[27] J.-M. Kelif, M. Coupechoux, and P. Godlewski, "A fluid model for performance analysis in cellular networks," *EURASIP J. Wireless Commun. Netw.*, vol. 2010, pp. 1–11, Aug. 2010.

[28] F. Baccelli and B. Blaszczyszyn, *Stochastic Geometry and Wireless Networks, Volume I: Theory*. Hanover, MA, USA: Now, 2009.

[29] M. Haenggi, *Stochastic Geometry for Wireless Networks*, Cambridge, U.K.: Cambridge Univ. Press, 2013.
[30] M. Kuczma, *An Introduction to the Theory of Functional Equations and Inequalities: Cauchy's Equation and Jensen's Inequality*. Basel, Switzerland: Birkhauser, 2008.

Hui Zhang received the B.Eng. degree in applied mathematics and the Ph.D. degree in electrical engineering from Beijing University of Posts and Telecommunications, Beijing, China, in 2005 and 2010, respectively.

Since 2010, he has been a faculty member with the School of Electrical Information and Optical Engineering, Nankai University, Nankai, China. From 2013 to 2014, he was a Postdoctoral Scholar with the School of Electrical and Computer Science, University of Southampton, Southampton, U.K. In 2014, he joined in the China–Korea Young Scientist Exchange Program. His research interests include cellular networks and wireless communication theory.

Sheng Chen (M'90–SM'97–F'08) received the B.Eng. degree in control engineering from the East China Petroleum Institute, Dongying, China, in 1982; the Ph.D. degree in control engineering from the City University London, London, U.K., in 1986; and the D.Sc. degree from the University of Southampton, Southampton, U.K., in 2005.

From 1986 to 1999, he held research and academic appointments with The University of Sheffield, Sheffield, U.K.; The University of Edinburgh, Edinburgh, U.K.; and the University of Portsmouth, Portsmouth, U.K. Since 1999, he has been with Electronics and Computer Science, the University of Southampton, Southampton, U.K., where he is currently a Professor of intelligent systems and signal processing. He is also a Distinguished Adjunct Professor with King Abdulaziz University, Jeddah, Saudi Arabia. He is the author of over 500 research papers. His research interests include adaptive signal processing, wireless communications, modeling and identification of nonlinear systems, neural network and machine learning, intelligent control system design, and evolutionary computation methods and optimization.

Dr. Chen is a Fellow of the Institution of Engineering and Technology and an ISI highly cited researcher in engineering (March 2004). In 2014, he was elected as a Fellow of the United Kingdom Royal Academy of Engineering.

Liang Feng received the B.Eng. degree in applied physics from Dalian University of Technology, Dalian, China, in 2004. He is currently working toward the Master's degree with Nankai University, Nankai, China, in 2012.

From 2004 to 2012, he carried out electronic countermeasures research with the Luoyang Electronic Equipment Center, China. His research interests include cellular mobile communications.

Yifeng Xie received the B.S. degree in electronic and information engineering from Nanjing Forestry University, Nanjing, China, in 2011 and the M.S. degree in communication and information systems from Nankai University, Nankai, China, in 2014.

His research interests include stochastic geometry and heterogeneous networks.

Lajos Hanzo (F'08) received the Master's and D.Sc. degrees in electronics and the Doctor Honoris Causa from the Technical University of Budapest, Budapest, Hungary, in 1976 and 1983, respectively.

During his 38-year career in telecommunications, he has held various research and academic posts in Hungary, Germany, and the U.K. Since 1986, he has been with the School of Electronics and Computer Science, University of Southampton, Southampton, U.K., where he is the Chair in telecommunications. He has successfully supervised about 100 Ph.D. students. He is the author or coauthor of 20 John Wiley/IEEE Press books on mobile radio communications, totalling in excess of 10 000 pages, and of more than 1400 research entries on IEEE Xplore. Currently, he is directing a 100-strong academic research team, working on a range of research projects in the field of wireless multimedia communications sponsored by industry, the Engineering and Physical Sciences Research Council (EPSRC) U.K., the European Research Council's Advanced Fellow Grant, and the Royal Society's Wolfson Research Merit Award. He is an enthusiastic supporter of industrial and academic liaison, and he offers a range of industrial courses.

Dr. Hanzo has acted both as a Technical Program Committee Chair and as a General Chair of IEEE conferences, has presented keynote lectures, and has received a number of distinctions. He is a Governor of the IEEE Vehicular Technology Society. From 2008 to 2012, he was the Editor-in-Chief of the IEEE Press and a Chaired Professor with Tsinghua University, Beijing, China. His research is funded by the European Research Council's Senior Research Fellow Grant. He is a Fellow of the Royal Academy of Engineering, the Institution of Engineering and Technology, and the European Association for Research and Signal Processing.